Published in IET Microwaves, Antennas & Propagation
Received on 30th July 2010
Revised on 15th December 2010
doi: 10.1049/iet-map.2010.0362

Special Issue on RF/Microwave Communication Subsystems for Emerging Wireless Technologies

ISSN 1751-8725

Low insertion loss substrate integrated waveguide quasi-elliptic filters for V-band wireless personal area network applications

D. Zelenchuk V. Fusco

High Frequency Electronics Cluster, The Institute of Electronics, Communication and Information Technology, Queen's University of Belfast, Queen's Road, BT3 9DT, Belfast, Northern Ireland, UK
E-mail: d.zelenchuk@qub.ac.uk

Abstract: Novel V-band substrate integrated waveguide (SIW) filters have been presented. Design procedures for the filters synthesis and mechanisms providing quasi-elliptic response have been explained. The insertion loss of the filters has been measured below 2 dB with microstrip-to-SIW transitions being included.

1 Introduction

Nowadays millimetre-wave systems are used well beyond their traditional niche of military and space and have already penetrated consumer-oriented market through applications such as automotive radars and high-speed wireless networks. Among those applications special attention is attached to 60 GHz wireless networks. This is stimulated by the existence of up to 9 GHz unlicensed spectrum bandwidth between 57 and 66 GHz [1]. New systems exploiting this spectrum will respond to growing demand for short-range transmission of uncompressed high-definition (HD) audio and video content in real time with data rates of up to 3 Gb/s as required for wireless HD [2].

Integrated filters are an important part of such a system. However, it is difficult to achieve low insertion loss for a filter designed at these frequencies; additionally, a printed circuit board (PCB) compliant solution would be useful for cost minimisation of consumer applications. At V-band complementary metal oxide semiconductor microstrip filters exhibit relatively high insertion loss (more than 4 dB) [3] and can be affected by electromagnetic interference. As an alternative, PCB technology substrate integrated waveguide (SIW) has recently been proposed. A number of different devices have been implemented which demonstrate good performance [4–6]. A comprehensive review of state-of-the-art in SIW research is given in [7]. Furthermore, several V-band components have been designed with SIW technology [8–10].

An SIW filter demonstrated in [9] had 3 dB insertion loss at 61–63 and 15 dB return loss as well as out-of-band rejection of 25 and 15 dB for lower and upper stopbands, respectively. A multilayer SIW low temperature co-fired ceramic (LTCC) filter was reported in [10] with insertion loss of 2 dB and return loss of 16 dB at 57–64 GHz as well as out-of-band rejection of 33 and 25 dB for lower and upper stopbands at 3 GHz outside the passband. In [10], however, in order to achieve 2 dB insertion loss, an additional compensation circuit was implemented.

In this paper, we propose two different low-loss SIW filter topologies with quasi-elliptic characteristics manufactured on polytetrafluoroethylene-based PCB substrate TaclamPLUS [11]. The substrate offers lower loss tangent alternative to liquid crystal polymer (LCP) and LTCC at V-band and is suitable for millimetre-wave packaging. The main objective of this paper is to demonstrate simple V-band filter designs compliant with typical PCB process for a softboard. The design of the filters is discussed in Section 2. Then in Section 3 the measurement and the de-embedding procedures are detailed. Results are discussed in Section 4 and the summary is given in Section 5.

2 Design

2.1 Substrate integrated waveguide

SIWs largely preserve the well-known advantages of waveguide structures such as high-Q, robustness, moderate power handling, no radiation and low cross-talk. Besides, they are easily fabricated on PCBs using standard processing techniques.

SIWs are manufactured by plating metallic vias in a dielectric substrate while retaining metal, usually copper, cladding on the top and bottom of the structure, see Fig. 1. The resulting closed SIW geometry bears straightforward relation to an equivalent rectangular waveguide of effective width a_{eff} [12]

$$a_{\text{eff}} = a - 1.08\frac{d^2}{s} + 0.1\frac{d^2}{a} \tag{1}$$

where d is the diameter of the vias, s the spacing between them and a is the width of the SIW. Employing (1), one can design a rectangular waveguide prototype of a

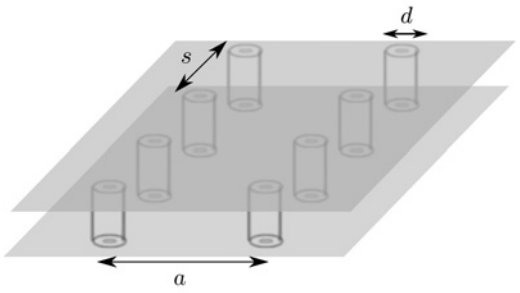

Fig. 1 *Substrate integrated waveguide*

circuit and then transfer it to SIW technology with minimal requirement for subsequent dimension refinement. Moreover, SIW scales with frequency with respect to the relative permittivity of the substrate ε_r as $(1/\sqrt{\varepsilon_r})$, that is, exactly as does a homogeneously filled rectangular waveguide.

The filters presented in this paper are designed at 0.200 mm Taconic TacLamPLUS substrate [11], with permittivity of 2.1 and loss tangent of 0.0008 specified at 50 GHz. This material is specifically developed for microwave packaging purposes as it permits ablation for creation of cavities into which microwave monolithic integrated circuit chips can be embedded, thus enabling implementation of system-on-substrate.

For the SIW filters developed in this paper, the diameter of all of the vias used has been set to 0.25 mm and their spacing is chosen as 0.4 mm. This agrees well with condition $d/s > 0.5$ ensuring that radiation loss is negligible [13]. Top metallisation of the substrate is 17-microns thick copper, and bottom metallisation is 1 mm thick copper. The bottom metallisation is kept intact in the etching process.

2.2 Microstrip-to-SIW transition

There is no standard measurement interface available for a standalone SIW structure and in order to measure them one needs to employ transitions to either coplanar waveguide (CPW) or microstrip line. The exponential microstrip-to-SIW transition reported in [5] was chosen in this work.

The dimensions of the taper were optimised in CST Microwave Studio to mate without discontinuity to a 70-micron wide microstrip line and to ensure minimal insertion loss in the passband of the filters at 57–66 GHz. As shown in Fig. 2, the return loss of the transition is better than 20 dB and the insertion loss is 0.5 dB over the band. Based on simulation, we estimate that the both transitions can add up to 1 dB insertion loss to the filters performance subject to their return loss.

2.3 Iris filter

A tremendous progress has recently been made with design of SIW filters for microwave and millimetre-wave frequencies [14–20]. However, most of the filters are designed at frequencies below 40 GHz, because of detrimental effect of manufacturing tolerances. Therefore in this paper, we employ simple filter topologies, which in our view are more robust with respect to manufacturing.

The first design presented here is a directly coupled resonator filter with inductive irises employed as coupling elements. Similar filters with single and double posts have been implemented in [5, 19]. For a bandpass filter with the resonators cascaded via K-inverters, normalised impedances of the inverters are given as follows [19]

$$\frac{K_{0,1}}{Z_0} = \sqrt{\frac{\pi}{2}\frac{\omega_\lambda}{g_0 g_1}}$$

$$\frac{K_{i,i+1}}{Z_0} = \frac{\pi}{2}\frac{\omega_\lambda}{\sqrt{g_j g_{j+1}}} \tag{2}$$

$$\frac{K_{n,n+1}}{Z_0} = \sqrt{\frac{\pi}{2}\frac{\omega_\lambda}{g_n g_{n+1}}}$$

where Z_0 is the waveguide impedance and ω_λ is the fractional bandwidth defined through guided wavelength at the edges λ_{g1}, λ_{g2} and the centre of the band λ_{g0} as

$$\omega_\lambda = \frac{\lambda_{g1} - \lambda_{g2}}{\lambda_{g0}}$$

The lowpass prototype filter parameters g corresponding particular transfer function can be found in [21].

Once the normalised impedances of the inverters have been found, the physical dimensions of corresponding inductive irises have to be obtained. For this procedure, we use the following method [19].

Each iris presents itself as a K-inverter, corresponding to the reactance X, see Fig. 3.

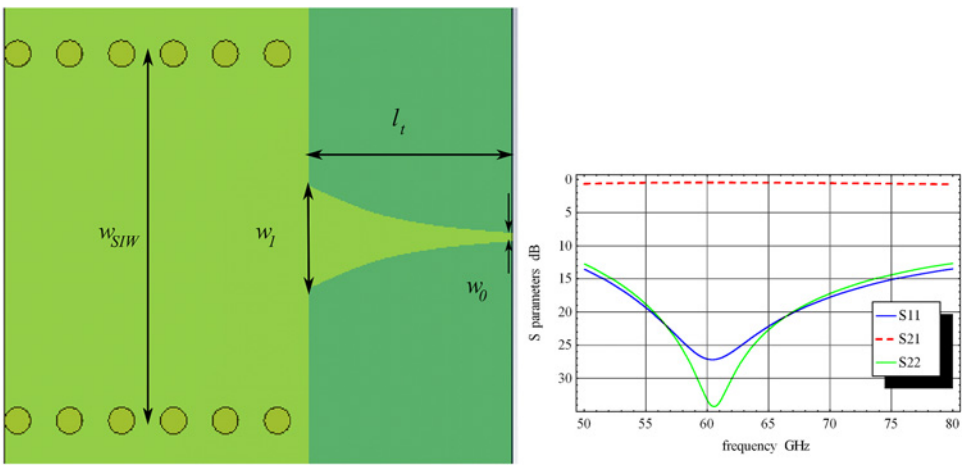

Fig. 2 *Microstrip-to-SIW transition and its performance ($w_{SIW} = 2.8$ mm, $w_1 = 0.78$ mm, $w_0 = 0.07$ mm and $l_t = 1.6$ mm)*

doi: 10.1049/iet-map.2010.0362

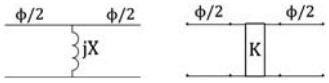

Fig. 3 *Model of inductive window in an SIW*

The parameters of the inverter are found from *S*-matrix of the element as

$$j\frac{X}{Z_0} = \frac{2S_{21}}{(1-S_{11})^2 - S_{21}^2}$$
$$\phi = -\tan^{-1}\left(\frac{2X}{Z_0}\right) \tag{3}$$
$$\frac{K}{Z_0} = \left|\tan\left(\frac{\phi}{2}\right)\right|$$

Once the inverter parameters are found, the distance between adjacent inductive windows can be evaluated as

$$l_i = \frac{\theta_i \lambda_{g0}}{2\pi}$$
$$\theta_i = \pi + \frac{1}{2}(\phi_i + \phi_{i+1}) \tag{4}$$

Following this synthesis procedure, an SIW bandpass Chebyshev filter with inductive irises can be designed.

In this paper, we use the procedure to design a three-pole Chebyshev filter with 0.1 dB insertion loss and 15 dB return loss in 57.36–65.76 GHz passband. First the inverter values K have been calculated using (2) as $K_{01} = K_{34} = 0.53$ and $K_{12} = K_{23} = 0.31$. Then dependencies of K and ϕ on width of the iris window in the SIW waveguide of width $a = 2.8$ mm have been computed by full-wave simulations of irises in Ansoft HFSS and then employing (3), see Fig. 4. The width values corresponding to the calculated K-values were found as $w_1 = 1.82$ mm and $w_2 = 1.5$ mm. Substituting the phase corresponding to the widths into (4) gives the distances between the irises as $l_1 = l_3 = 1.7$ and $l_2 = 1.57$. These values have been taken as a first approximation and then tuned in order to minimise the return loss in the passband.

The resulting physical layout for the filter together with its *S*-parameters simulated in Ansoft HFSS is shown in Fig. 5. The dimensions of the filter are $l_1 = l_3 = 1.65$ mm, $l_2 = 1.6$ mm, $w_1 = 1.76$ and $w_2 = 1.47$. The insertion loss is less than 1 dB. The rejection roll-off properties of the filter at higher frequencies are relatively poor.

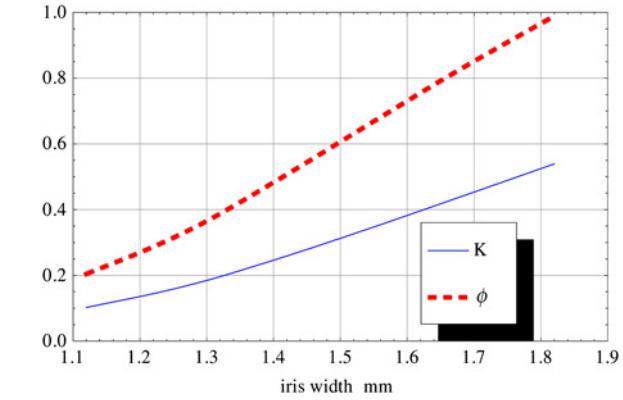

Fig. 4 *Normalised inverter impedance and phase against iris width*

To improve the stopband response, an additional stub producing a transmission zero is introduced into the design, see Fig. 6. The stub is itself a highly dispersive inverter that has transmission zeros. Such inverters can be incorporated into a synthesis procedure for direct-coupled resonator filters, as the one presented above [22]. There is a simpler alternative approach which is to synthesise an inverter with an impedance equal to 1 in the passband and transmission zeros in the stopband. Such a stub can be added to an existing filter to improve its stopband performance. With this approach in mind, the stub dimensions were optimised by numerical simulations as $w_s = 2.8$ mm and $l_s = 5.4$ mm.

As shown in Fig. 6, the stub introduces three transmission zeros at 50, 68 and 79 GHz and its normalised impedance exceeds 0.85 in the passband and phase is close to $-\pi/2$. Therefore upon properly adjusting the length of the connecting waveguide section, one can combine the iris filter with the stub section in order to improve the stopband response of the filter while almost not compromising its passband performance. It has to be noted that the transfer function of the filter is not Chebyshev anymore. The length of the connecting section was accordingly adjusted to $l_o = 1.1$ mm. The resultant filter with microstrip-to-SIW transitions attached and its *S*-parameters are simulated in Ansoft HFSS are shown in Fig. 7.

The filter has a sharp roll-off and wide stopband covering the 68–80 GHz range with out-of-band rejection better than 10 dB and transmission zeros at 68 and 80 GHz. Despite overall improvement, rejection at 78 GHz has risen from 12 to 10 dB, which is due to a mismatch caused by the stub. The composite insertion loss is less than 1.7 dB within the passband. The increase in the insertion loss is attributed to the microstrip-to-SIW transitions.

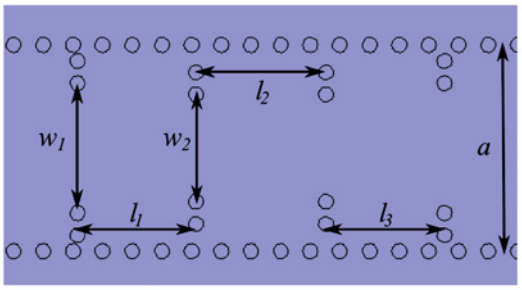

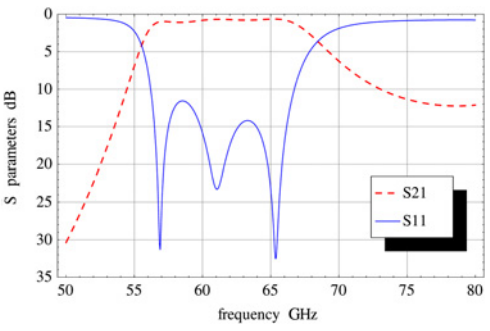

Fig. 5 *Bandpass SIW filter*

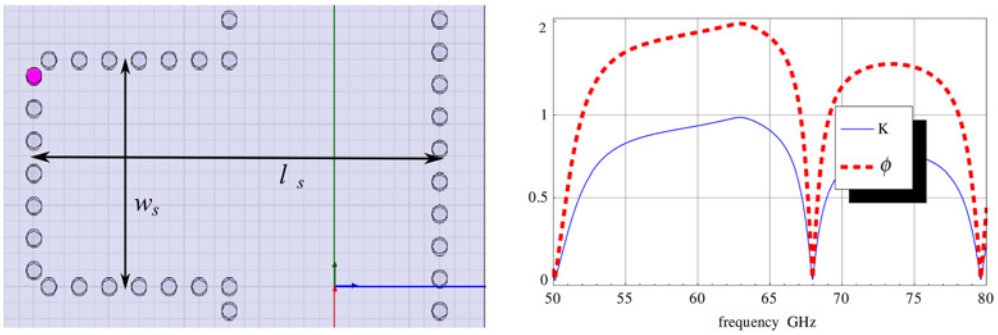

Fig. 6 *SIW stub and its normalised inverter impedance and phase for $w_s = 2.8$ mm and $l_s = 5.4$ mm*

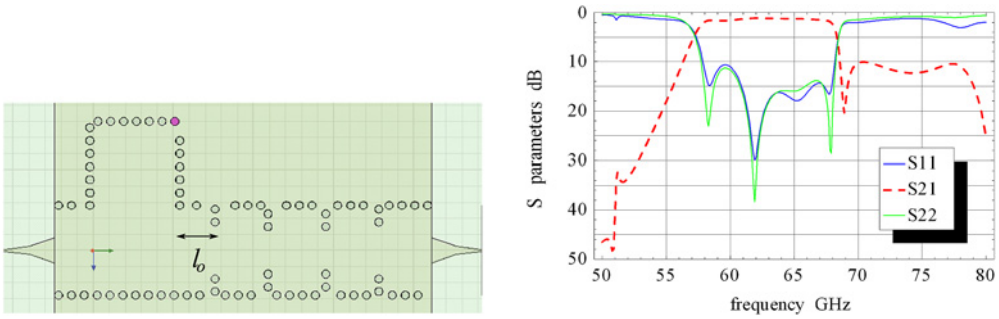

Fig. 7 *Bandpass filter with enhanced stopband and microstrip launch ports, $l_o = 1.1$ mm*

2.4 Cavity filter

The second design suggested in this paper is a filter with an over-moded cavity, see Fig. 8. The design of the filter is based on the multi-mode cavity filters techniques reported in [23–25]. A rigorous design procedure that prescribes the positions of the poles and transmission zeros through a coupling matrix synthesis for multi-mode cavities is presented in [24]. However, the approach requires substantial full-wave simulation in order to synthesise appropriate inter-cavities mode couplings as well as source and load coupling to the modes. The procedure involves multi-parametric tuning, which for small number of cavities is straightforward if the optimisation technique proposed in [23] is followed, with the additional constraint that in this paper we enforce realistic technology restrictions that will be encountered at the fabrication stage.

At the initial design stage, the preliminary dimensions of the cavities were chosen and subsequently the entire structure is optimised to provide the required spectral response, taking into account the equivalence of a SIW and a rectangular waveguide. The equivalent structure was optimised in the Microwave Wizard waveguide simulator, [26], with the aim of ensuring 0.1 dB insertion loss and 15 dB return loss in the same passband as previous filter. The first approximation for the cavity dimensions were taken as $w_3 = w_6 = 6.9$ mm and $l_2 = l_3 = 1.85$ mm in order to ensure that both TE_{101} and TE_{102} modes are resonant in

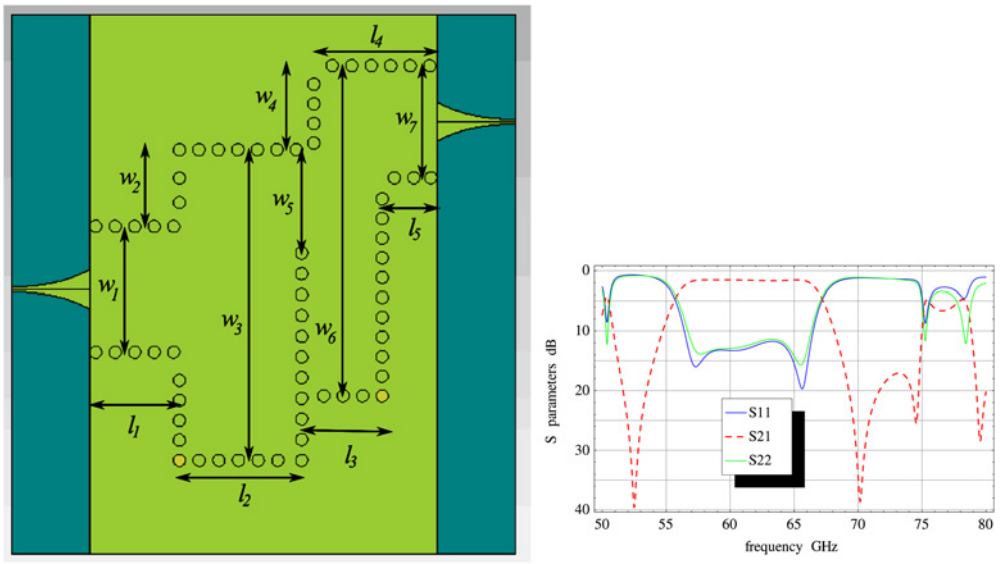

Fig. 8 *Cavity filter design and simulated performance*

doi: 10.1049/iet-map.2010.0362

the passband. To reduce the sensitivity of the filter response to the PCB manufacturing process, several topology restrictions were enforced. First, the inter-cavity wall has been implemented with single row of vias of exactly the same diameter as all other vias in the design. Second, the iris in the wall is located at the side of the wall; this reduces the number of objects in this sensitive area. Finally, input and output irises are of the same dimensions as the corresponding SIW waveguide sections. The position and dimensions of the coupling irises are optimised that the transmission zeros appear both in the lower and the upper stopband. Then, with the aid of (1), the design was transferred to SIW PCB and simulated in CST Microwave Studio.

As a result, the dimensions of the filter were set as follows: $w_1 = 2.55$ mm, $w_2 = 1.56$ mm, $w_3 = 6.32$ mm, $w_4 = 1.71$ mm, $w_5 = 2.11$ mm, $w_6 = 6.71$ mm, $w_7 = 2.25$ mm, $l_1 = 1.84$ mm, $l_2 = 1.84$ mm, $l_3 = 1.65$ mm, $l_4 = 2.5$ mm and $l_5 = 1.12$ mm.

The response of the filter is presented in Fig. 8. The insertion loss including launch transitions is better than 1.7 dB in the 57–66 GHz passband and the stopbands measured at −10 dB level cover 52–55 GHz and 68–75 GHz bands. The latter has been achieved due to placement of transmission zeros at 53, 70 and 74 GHz in the optimisation goal function.

Owing to the above-mentioned geometry restriction, the optimised filter has two resonant nodes in the first cavity and one in the second. The transmission zeros in the stopband are the consequence of the destructive interference between different modes coexisting in the filter cavities at the ports and/or cavity interfaces. The first transmission zero in the lower stopband appears as result of negative coupling between the resonant nodes, and the transmission zeros in the upper stopband are the result of interference of the higher order modes.

The spurious transmission bands in near 50 and 75 GHz are not of concern in this paper, since the filter is designed to be part of an integrated front-end where active components will not be operating at the frequencies. Yet, the authors realise it can be of concern for some application and will attempt to improve it in the future work.

3 Measurement

3.1 Measurement setup

The structures were measured using a cascade millimetre-wave probe station with 50 Ω ground-signal-ground (GSG) probes. The pitch of the probes is 150 microns. The probes before each measurement were calibrated using an automated line-line-reflect-match (LLRM)-procedure at the probe station and the calibration error was below 0.1 dB for the entire frequency range from 50 to 80 GHz.

3.2 De-embedding

To the interface to GSG probes, the circuits were terminated at the coplanar waveguide with ground plane (CPWG) probe pads, see Fig. 9. The dimensions of the pads were chosen to comply with PCB etching process restriction of 70 microns on the smallest feature dimension and the 150-micron pitch of the 50 Ω GSG probe. The microstrip line width in the transition is 70 microns, the gap width is 80 microns, the diameter of via is 250 microns and the area of each pad is 1 mm × 0.45 mm.

Fig. 9 *CPWG-microstrip transition and transmission line calibration set*

The chosen dimensions do not ensure good matching to the probe since neither CPWG nor microstrip line impedance is 50 Ω, indeed for the dimensions used they are 100 and 135 Ω, correspondingly. Hence a robust de-embedding procedure has to be applied in order to exclude the effect that these pads have on measurement results.

To de-embed the CPWG-microstrip transitions, an adaption of the method reported in [27] has been employed. The method is based on extracting the ABCD-matrix of the transition by measuring two uniform transmission lines of different length terminated with transitions.

Two microstrip lines 6 and 7 mm long terminated with transitions have been fabricated and measured, see Fig. 9. Each of the calibration samples is described by *ABCD*-matrix as follows [27]

$$\begin{pmatrix} A & B \\ C & D \end{pmatrix}_{\text{cal}} = \begin{pmatrix} \alpha & \beta \\ \delta & \varepsilon \end{pmatrix} \begin{pmatrix} \cos(\gamma l) & Z_0 \sin(\gamma l) \\ Z_0^{-1} \sin(\gamma l) & \cos(\gamma l) \end{pmatrix} \times \begin{pmatrix} \varepsilon & \beta \\ \delta & \alpha \end{pmatrix}$$

where γ is the complex propagation constant, l is the length of the uniform transmission line and $\begin{pmatrix} \alpha & \beta \\ \delta & \varepsilon \end{pmatrix}$ is the *ABCD*-matrix of the CPWG-microstrip transition. Following the approach given in [27], the *ABCD*-matrices of the transitions have been found. Unfortunately, the analytical LC-circuit derived from the *ABCD*-matrix in [16] fails to account for the loss in the pads, and consequently, the *ABCD*-matrices of the transitions themselves are used.

The measured transmission matrix of the device under test (DUT) with the transitions reads as

$$\begin{pmatrix} A & B \\ C & D \end{pmatrix}_{\text{DUT+pads}} = \begin{pmatrix} \alpha & \beta \\ \delta & \varepsilon \end{pmatrix} \begin{pmatrix} A & B \\ C & D \end{pmatrix}_{\text{DUT}} \begin{pmatrix} \varepsilon & \beta \\ \delta & \alpha \end{pmatrix}$$

The de-embedded transmission matrix of the DUT can then be found as

$$\begin{pmatrix} A & B \\ C & D \end{pmatrix}_{\text{DUT}} = \begin{pmatrix} \alpha & \beta \\ \delta & \varepsilon \end{pmatrix}^{-1} \begin{pmatrix} A & B \\ C & D \end{pmatrix}_{\text{DUT+pads}} \begin{pmatrix} \varepsilon & \beta \\ \delta & \alpha \end{pmatrix}^{-1}$$

To illustrate the effect of the procedure, the *S*-parameters of the 6 mm transmission line with pads and de-embedded are presented in Fig. 10.

As one can see from Fig. 10, the return loss is better than 25 dB across the frequency range, confirming that the DUT is a well-matched transmission line. The difference between S11 and S22 in both plots might be attributed to the probe positioning uncertainty and manufacturing tolerances.

The same factors contribute to numerical errors of the de-embedding, resulting in the kinks of insertion loss in the range between 61 and 65 GHz persistently manifested for all the measured calibration samples. The effect is too big to be a measurement calibration error, which was known to be below 0.1 dB across the band. Our studies have shown

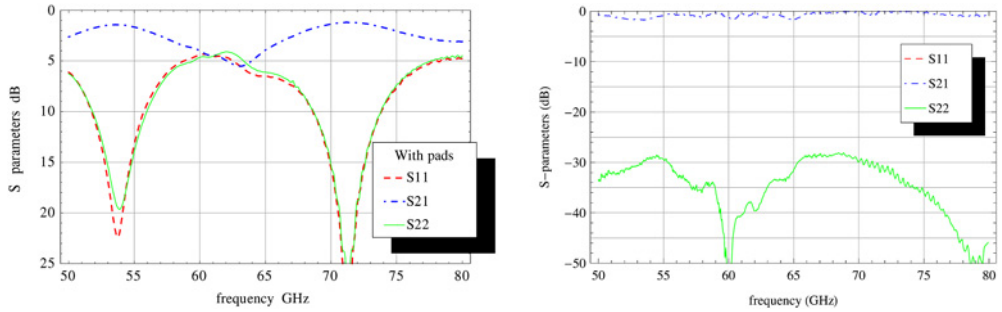

Fig. 10 *S-parameters of 6 mm long microstrip line: before and after de-embedding*

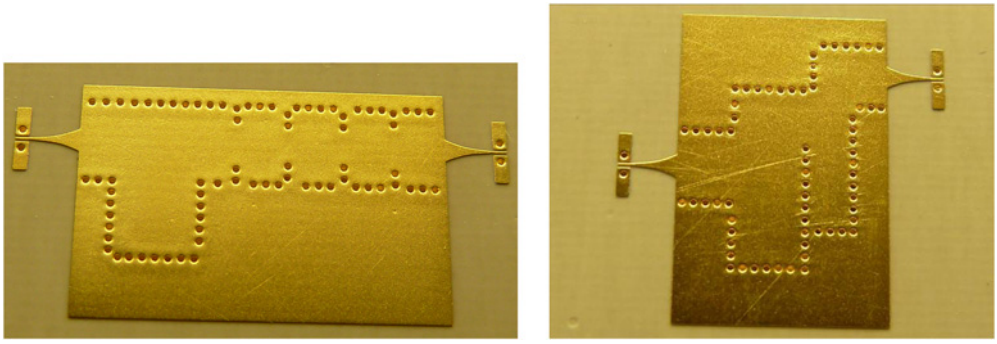

Fig. 11 *Manufactured filters*

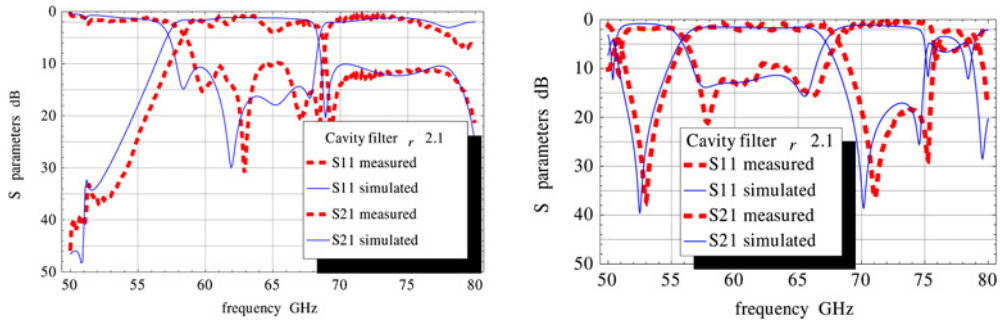

Fig. 12 *Comparison of measured and simulated performance for the iris filter and the cavity filter with permittivity of 2.1*

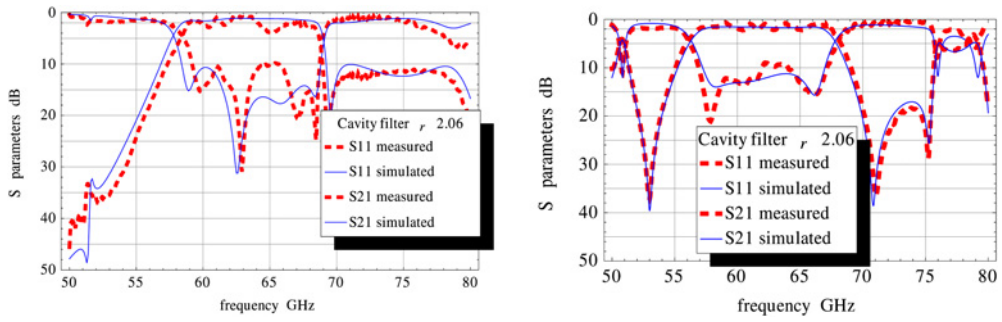

Fig. 13 *Comparison of measured and simulated performance for the iris filter and the cavity filter with permittivity of 2.06*

that the effect can be reduced if one has to enforce the *S*-matrix symmetry of the calibration samples. Unfortunately, both calibration samples satisfy resonant conditions at the frequency range, which enhances the numerical error. Also, one has to remember that the method implies identity of all the transitions, which is not true due

doi: 10.1049/iet-map.2010.0362

to the manufacturing tolerances. Thus, the de-embedding error can accumulate at particular frequencies and cancel out at the others. This error influences all the de-embedded results presented below. Therefore when the insertion loss is estimated the artefact is discarded.

4 Results

The manufactured filters are presented in Fig. 11. The filters were measured and the results were de-embedded according to the method described above. As shown in Fig. 12, the responses of both filters are shifted towards lower than predicted frequencies when compared with results simulated for the substrate with permittivity of 2.1. In fact both manufacturing and permittivity tolerances can contribute to the shift of passband; below we have attempted to correct the latter as it is major factor in our view. Bearing in mind the scaling properties of SIW with respect to permittivity discussed in Section 2, the actual material permittivity was estimated to be 2.06 by fitting the positions of transmission zeros in the responses. Simulations with this value of permittivity were performed and the results were compared with the experimental ones in Fig. 13. For both filters, the experimental results are in a very good agreement with the simulations for the adjusted value of the permittivity.

In view of the explanation of the insertion loss kinks in the passband given in Section 3, one can conclude that the overall insertion loss in the passband is better than 2 dB for both filters.

5 Conclusions

Two novel V-band filters with quasi-elliptic responses have been presented in this paper. Design procedures for the filters synthesis, physical mechanisms providing quasi-elliptic response and de-embedding of the measured results have been explained. The insertion loss of the filters is measured below 2 dB when microstrip-to-SIW transitions are included. The return loss in passband is measured below 10 dB, which is to be improved in future work. The filters have sharp roll-off due to the transmission zeros and the out-of-band rejection in the upper stopband of 10 and 17 dB. Both filters can be used as an advanced packaging solution for V-band wireless personal network front-end applications.

6 Acknowledgments

The authors greatly appreciate suggestions given by reviewers. This work was supported by the Engineering and Physical Sciences Research Council (U.K.) under EPSRC Grant EP/E01707X/1 and by Northern Ireland Department for Employment and Learning under 'Strengthening All Island–Mobile Wireless Futures' research program. Authors wish to thank Taconic International Ltd., Mullingar, Ireland for support and provided materials, and Varioprint AG, Heiden, Switzerland for fabrication of the circuits. Authors also wish to acknowledge stimulating discussions and advice provided by Dr George Goussetis.

7 References

1 http://www.ecma-international.org/publications/files/ECMA-ST/ECMA-387.pdf
2 http://www.wirelesshd.org/
3 Liu, C.-H., Hsu, C.-Y., Chen, C.-Y., Chuang, H.-R.: '60-GHz bandpass filter with ACMRC resonator fabricated using 0.18-μm CMOS technology', *Microw. Opt. Technol. Lett.*, 2009, **51**, pp. 597–600
4 Zhong, C., Xu, J., Yu, Z., Li, J.: 'Miniaturized antenna using half-mode substrate integrated waveguide structure', *Microw. Opt. Technol. Lett.*, 2008, **50**, pp. 3214–3218
5 Sotoodeh, Z., Biglarbegian, B.: 'A novel bandpass waveguide filter structure on SIW technology', *Progr. Electromagn. Res. Lett.*, 2008, **2**, pp. 141–148
6 Xu, F., Wu, K.: 'Periodic leaky-wave antenna for millimeter wave applications based on substrate integrated waveguide', *IEEE Trans. Antennas Propag.*, 2010, **58**, pp. 340–347
7 Bozzi, M., Perregrini, L., Wu, K., Arcioni, P.: 'Current and future research trends in substrate integrated waveguide technology', *Radioengineering*, 2009, **18**, pp. 201–209
8 Lai, Q., Fumeaux, C., Hong, W., Vahldieck, R.: '60 GHz aperture-coupled dielectric resonator antennas fed by a half-mode substrate integrated waveguide', *IEEE Trans. Antennas Propag.*, 2010, **58**, pp. 1856–1864
9 Tokuda, K.: 'A V-band planar narrow bandpass filter using a new type integrated waveguide transition', *IEEE Microw. Wirel. Compon. Lett.*, 2004, **14**, pp. 545–547
10 Lee, G., Yoo, C., Kim, Y., Kim, J., Park, Y., Yook, J.: 'A 60 GHz embedded SIW (substrate integrated waveguide) BPF considering the transition effect'. IEEE Asia Pacific Microwave Conf., Singapore, 2009, pp. 1192–1195
11 http://www.taconic-add.com/pdf/taclamplus.pdf
12 Xu, F., Wu, K.: 'Guided-wave and leakage characteristics of substrate integrated waveguide', *IEEE Trans. Microw. Theory Tech.*, 2005, **53**, pp. 66–73
13 Bozzi, M., Perregrini, L.: 'Modeling of conductor, dielectric, and radiation losses in substrate integrated waveguide by the boundary integral-resonant mode expansion method', *IEEE Trans. Microw. Theory Tech.*, 2008, **56**, pp. 3153–3161
14 Chen, X.-P., Wu, K.: 'Self-equalised pseudo-elliptical filter made of substrate integrated waveguide', *Electron. Lett.*, 2009, **45**, pp. 112–113
15 Chuang, C.-C., Lin, H.-H., Wang, C.-L.: 'Design of dual-mode SIW cavity filters'. IEEE Region 10 Conf. TENCON, October 2007, pp. 1–4
16 Chen, X., Hong, W., Hao, Z., Wu, K.: 'Substrate integrated waveguide quasi-elliptic filter using extracted-pole technique'. Proc. Asia-Pacific Conf., 2005, p. 3
17 Wei, Q.-F., Li, Z.-F., Li, L., Zhang, W.-J., Mao, J.-F.: 'Three-pole cross-coupled substrate-integrated waveguide bandpass filters based on PCB process and multilayer LTCC technology', *Microw. Opt. Technol. Lett.*, 2009, **51**, pp. 71–73
18 Dong, Y., Hong, W., Tang, H., Chen, J., Wu, K.: 'Planar realization of a Q-band triple-mode filter using high-order resonances', *Microw. Opt. Technol. Lett.*, 2009, **51**, pp. 600–603
19 Deslandes, D., Wu, K.: 'Millimeter-wave substrate integrated waveguide filters'. IEEE CCECE Canadian Conf. on Electrical and Computer Engineering, Montreal, 2003, pp. 1917–1920
20 Zhang Cheng, H., Wei, H., Xiao Ping, C., Ji Xin, C., Ke, W., Tie Jun, C.: 'Multilayered substrate integrated waveguide (MSIW) elliptic filter', *IEEE Microw. Wirel. Compon. Lett.*, 2005, **15**, pp. 95–97
21 Hong, J., Lancaster, M.: 'Microstrip filters for RF/microwave applications' (Wiley, New York, 2001)
22 Amari, S., Bornemann, J.: 'Using frequency-dependent coupling to generate finite attenuation poles in direct-coupled resonator bandpass filters', *IEEE Microw. Guided Wave Lett.*, 1999, **9**, pp. 404–406
23 Guglielmi, M., Jarry, P., Kerherve, E., Roquebrun, O., Schmitt, D.: 'A new family of all-inductive dual-mode filters', *IEEE Trans. Microw. Theory Tech.*, 2001, **49**, pp. 1764–1769
24 Rosenberg, U., Amari, S.: 'Novel design possibilities for dual-mode filters without intracavity couplings', *IEEE Microw. Wirel. Compon. Lett.*, 2002, **12**, pp. 296–298
25 Chen, X.-P., Wu, K., Drolet, D.: 'Substrate integrated waveguide filter with improved stopband performance for satellite ground terminal', *IEEE Trans. Microw. Theory Tech.*, 2009, **57**, pp. 674–683
26 'Mician Microwave Wizard, http://www.mician.com/cms/content/products/wave_wizard', accessed April 2011
27 Torres-Torres, R., Hernandez-Sosa, G., Romo, G., Sanchez, A.: 'Characterization of electrical transitions using transmission line measurements', *IEEE Trans. Adv. Packag.*, 2009, **32**, pp. 45–52